

Inhibition of CDK4/6 by Palbociclib Significantly Extends Survival in Medulloblastoma Patient-Derived Xenograft Mouse Models



Michelle L. Cook Sangar¹, Laura A. Genovesi², Madison W. Nakamoto¹, Melissa J. Davis³, Sue E. Knobluagh⁴, Pengxiang Ji², Amanda Millar², Brandon J. Wainwright², and James M. Olson¹

Abstract

Purpose: Bioinformatics analysis followed by *in vivo* studies in patient-derived xenograft (PDX) models were used to identify and validate CDK 4/6 inhibition as an effective therapeutic strategy for medulloblastoma, particularly group 3 MYC-amplified tumors that have the worst clinical prognosis.

Experimental Design: A protein interaction network derived from a *Sleeping Beauty* mutagenesis model of medulloblastoma was used to identify potential novel therapeutic targets. The top hit from this analysis was validated *in vivo* using PDX models of medulloblastoma implanted subcutaneously in the flank and orthotopically in the cerebellum of mice.

Results: Informatics analysis identified the CDK4/6/CYCLIN D/RB pathway as a novel "druggable" pathway for multiple subgroups of medulloblastoma. Palbociclib, a highly specific inhibitor of CDK4/6, was found to inhibit RB phosphorylation and cause G₁ arrest in PDX models of medulloblastoma. The drug caused rapid regression of Sonic hedgehog (SHH) and MYC-amplified group 3 medulloblastoma subcutaneous tumors and provided a highly significant survival advantage to mice bearing MYC-amplified intracranial tumors.

Conclusions: Inhibition of CDK4/6 is potentially a highly effective strategy for the treatment of SHH and MYC-amplified group 3 medulloblastoma. *Clin Cancer Res*; 23(19); 5802–13. ©2017 AACR.

Introduction

Medulloblastoma is the most common malignant brain tumor in children. Because of advances in cancer care over the last 20 years, 70% of patients diagnosed with medulloblastoma are cured of their disease using treatments that include surgery, multiagent cytotoxic therapy, and craniospinal radiation (1). However, these therapies are associated with significant long-term toxicities in surviving patients, including neurocognitive impairment, endocrinopathy, and secondary malignancy (1–3). In addition, there are few effective therapies available for patients with high-risk disease or tumors that recur following standard-of-care therapy and these patients have a poor prognosis.

One approach to increase the cure rate and decrease the incidence of long-term toxicities is to use therapies that are

targeted specifically to the biology of the tumor and spare normal tissues. Numerous transcriptional profiling studies have been performed to investigate the signaling pathways that underlie the pathogenesis of medulloblastoma (4–9). Based upon these studies a general consensus has been reached that there are four major subgroups of medulloblastoma, WNT, SHH, group 3, and group 4, which demonstrate distinct characteristics regarding patient demographics, histology, genetic profile, and clinical outcome (10). WNT and SHH subgroups are named after the signaling pathway that plays a predominant role in their pathogenesis, whereas the molecular drivers of group 3 and 4 subgroups are currently unknown (10). Approximately 11% to 17% of group 3 tumors harbor MYC amplification (5, 11, 12) and patients with this tumor subtype have the worst prognosis (5, 9, 10). It is therefore of the utmost importance that molecular drivers of this subgroup are identified to improve patient outcomes.

In our (L.A. Genovesi, M.J. Davis, and B.J. Wainwright) previous work, a *Sleeping Beauty* (SB) mutagenesis approach was performed to identify candidate cancer genes that function as novel drivers of medulloblastoma (13). An inducible SB transposon system was introduced into the *Patched1*-heterozygous (*Ptch1*^{lacZ/+}) mouse model of SHH-driven medulloblastoma to identify genes that functionally cooperate with SHH signaling to promote tumorigenesis. The resulting tumors were confirmed as medulloblastoma by histopathologic analysis (13). Sequencing revealed common insertion sites (CIS) for the transposon in 56 protein-coding genes, highlighting these CIS-derived candidate genes as potential drivers of tumorigenesis in the *Ptch1* mouse model. Cross-species comparative analysis was performed

¹Clinical Research Division, Fred Hutchinson Cancer Research Center, Seattle, Washington. ²Institute for Molecular Bioscience, The University of Queensland, St. Lucia, Queensland, Australia. ³Walter and Eliza Hall Institute of Medical Research, Parkville, Victoria, Australia. ⁴Department of Veterinary Biosciences, College of Veterinary Medicine, The Ohio State University, Columbus, Ohio.

Note: Supplementary data for this article are available at Clinical Cancer Research Online (<http://clincancerres.aacrjournals.org/>).

M.L. Cook Sangar and L.A. Genovesi contributed equally to this article.

Corresponding Author: James M. Olson, Fred Hutchinson Cancer Research Center, 1100 Fairview Avenue North, D4-100, Seattle, WA 98109. Phone: 206-667-7955; E-mail: jolson@fredhutch.org

doi: 10.1158/1078-0432.CCR-16-2943

©2017 American Association for Cancer Research.

Translational Relevance

Medulloblastoma is the most common malignant brain tumor in children. The disease is classified into four subgroups that vary considerably with regard to patient prognosis. The ideal drugs to advance to clinical trials are those with relevance to multiple subclasses with priority given to agents that show activity in poor prognosis subgroups. We used bioinformatics analysis to identify the CDK4/6/CYCLIN D/RB pathway as a novel therapeutic target in multiple medulloblastoma subgroups, and demonstrated significant therapeutic benefit of palbociclib, a CDK 4/6 inhibitor, in both Sonic hedgehog and group 3 patient-derived xenografts (PDX) of medulloblastoma. Our most striking result is the dramatic survival benefit that palbociclib confers on mice bearing two different PDX MYC-amplified group 3 medulloblastomas, which are known to have the worst clinical prognosis. The data presented were used to launch a phase I clinical trial to test safety of palbociclib in pediatric patients with central nervous system tumors.

whereby human orthologs of the candidate genes identified from this screen were used to select corresponding probes from a previously published expression analysis of human medulloblastoma. CIS-derived candidate cancer genes and their local protein interaction networks accurately defined all four molecular subgroups of medulloblastoma. Combined, these findings suggest that the CIS-derived candidate cancer genes and associated protein networks disrupted by *SB* transposon mutagenesis were highly relevant to the biology underlying all subgroups of medulloblastoma and thereby represent a number of therapeutic avenues for intervention common to medulloblastoma subgroups.

In the current study, the associated protein network for one of our previously identified top ranked CIS-candidate protein coding genes, *cyclin-dependent kinase Inhibitor 2A* (*Cdkn2a*; ref. 13), was interrogated to identify novel drug targets for medulloblastoma. This analysis identified the CDK4/6/Cyclin D/Rb pathway as a "druggable" pathway for all non-WNT medulloblastomas. *CDKN2A* is a tumor suppressor gene encoding the Cyclin-dependent kinase inhibitor 2A protein (p16), that functions to inhibit cyclin-dependent kinases 4 and 6 (CDK4/6; ref. 14). These highly homologous enzymes play a key role in regulating cell-cycle progression through the G₁-S transition. They each form an active complex with a D-type CYCLIN and catalyze the phosphorylation of the retinoblastoma (RB) protein (15–17). Hyperphosphorylation of RB leads to release of its binding partner, E2F, and activates transcription of genes required for entry into S-phase and commitment to cell division (15).

Mutations in the CDK4/6/CYCLIN D/RB pathway that result in loss of RB function have been shown to be important for medulloblastoma tumor development and signify a poor survival outcome for patients (12, 18–20). In particular, engagement of this pathway has been shown to be the mechanism of tumor progression in preclinical *Ptch1*-mutant mice consistent with the finding that CDK6 amplification and *CDKN2A/B* deletion were among the most common genomic alterations that alter core signaling pathways in SHH-driven medulloblastoma (12, 21). Transgenic *p53*-null mice that have either somatic inactivation of

Rb in the external granular layer of the developing cerebellum (18) or germline loss of *Cdkn2c* (19) have a high incidence of spontaneous medulloblastoma formation. In addition, genomic studies have identified *CDK6* as one of the most common recurrent high-level amplifications in SHH, group 3, and group 4 medulloblastoma (12), and *CDK6* overexpression is an independent prognostic indicator for poor overall survival in patients (20). Therefore, multiple lines of evidence implicate the CDK4/6/CYCLIN D/RB pathway as a driver of medulloblastoma tumorigenesis. Mutant RB has not been observed in medulloblastoma, so therapies that restore appropriate regulation of RB function and activate the G₁-S checkpoint control may be an effective therapeutic strategy that is broadly applicable to all subgroups.

Palbociclib (IBRANCE, Pfizer, Inc.) is a selective inhibitor of CDK4/6 that functions to prevent RB hyperphosphorylation and arrest cells in the G₁ phase of the cell cycle (22). It has demonstrated efficacy in a variety of RB-positive tumors, including several different types of brain tumors namely glioblastoma multiforme and diffuse intrinsic pontine glioma (22–25), and has been FDA-approved as part of a combination therapy for advanced breast cancer. The selectivity of palbociclib for CDK4/6 is thought to provide a therapeutic window by preferentially targeting RB-driven tumor cells compared with most proliferating noncancerous cells (26, 27).

Because the CDK4/6/CYCLIN D/RB pathway has been identified as a vulnerable pathway in medulloblastoma, we tested the efficacy of palbociclib as a single agent in the treatment of patient-derived xenograft (PDX) mouse models in an effort to identify a novel effective therapeutic regimen for patients with medulloblastoma.

Materials and Methods

Animals

Four- to 6-week-old, approximately 20 g, female Hsd:ATHymic Nude-*Foxn1*^{nu} (athymic nude) mice (Envigo) and 6- to 10-week-old, approximately 18 to 34 g, male NOD.Cg-*Prkdc*^{scid}*Il2rg*^{tm1Wjl}/*SzJ* (NSG) mice (The Jackson Laboratory) were housed in a barrier facility with food and water provided *ad libitum* on a 12-hour light/dark cycle, in accordance with the NIH Guide for the Care and Use of Experimental Animals with approval from Fred Hutchinson Institutional Animal Care and Use Committee (IR#1457) or the University of Queensland Molecular Biosciences Committee (IMB/360/15).

PDX medulloblastoma mouse models

Studies were conducted in three PDX medulloblastoma mouse models, Med-211FH, Med-411FH, and Med-1712FH generated in the Olson laboratory using pediatric patient tumor tissue obtained from Seattle Children's Hospital with approval from the Institutional Review Board. Med-211FH is a MYC-amplified Group 3 medulloblastoma with classic morphology from a 2.8-year-old patient. Med-411FH is a MYC-amplified Group 3 medulloblastoma with large cell/anaplastic morphology from a 3-year-old patient. Med-1712FH is an SHH medulloblastoma with Desmoplastic/nodular morphology from a 4.9-year-old patient. Tissue was first xenografted into mice within hours of surgical removal from the patient, and passaged exclusively in immunocompromised mice (NSG or athymic nude). Xenografted tumors were subjected to genomic analysis and compared with the primary tumor.

Flank and orthotopic xenografts

Tissue was harvested from intracranial tumors in symptomatic donor mice and processed in serum-free DMEM or PBS by trituration through an 18-g needle. The cells were filtered, centrifuged, and resuspended in serum-free DMEM or PBS. For subcutaneous xenografts, cells were suspended at a concentration of 25,000–50,000/μL and diluted 1:1 with Matrigel. Two-hundred microliters of cell suspension ($2.5\text{--}5 \times 10^6$ cells) was injected subcutaneously in flanks of athymic nude (Med-211FH) and NSG (Med-1712FH) mice. For orthotopic xenografts, athymic nude mice were anesthetized and an incision was made to expose the skull. A hole was created in the calvarium above the right cerebellar hemisphere, 2-mm lateral (right) to the sagittal suture, 2-mm posterior of the lambdoid suture, using a microdrill (0.9-mm burr). Two microliters of Med-211FH or Med-411FH cell suspension (100,000 cells) was injected into the brain parenchyma approximately 2-mm under the dura. The burr hole site was filled with SurgiFoam and the incision was closed with tissue glue.

In vivo chemotherapy

Palbociclib isethionate (Pfizer) was used for experiments with Med-211FH and Med-411FH; palbociclib hydrochloride (Selleckchem) was used for experiments with Med-1712FH. Palbociclib was dissolved in 50 mmol/L sodium lactate, pH 4 and administered orally daily at 120 mg/kg, unless otherwise stated. An equivalent volume of 50 mmol/L sodium lactate, pH 4 was administered orally daily to mice in vehicle groups.

In vivo efficacy studies

Subcutaneous tumors. Efficacy studies were conducted using Med-211FH and Med-1712FH subcutaneous tumors between 200 and 700 mm³ in size. One Med-211FH tumor was enrolled at 1,200 mm³ in the pilot study. Mice were stratified into groups according to tumor size and randomly assigned to palbociclib or vehicle treatment. Treatment was administered for 16 to 28 days. Tumor volume and mouse weights were recorded every 2 to 4 days. Tumors were measured with calipers and tumor volume was calculated: tumor volume (mm³) = [(length × width²)/2].

Protocol alterations introduced in the Med-211FH definitive efficacy study include: rolling enrollment with 4 cohorts; use of Study Advantage (Tumor Tracker, LLC) software to track tumor volume [(Length × Width² × 3.14159)/6] and mouse weights; dose reduction to 75 mg/kg following studies demonstrating equivalent rate and extent of tumor regression as compared with 120 mg/kg. The 75 mg/kg dose was also used in Med-1712FH studies.

Orthotopic tumors. Once brain tumor growth was confirmed by histology or development of symptoms in a subset of mice, all mice were enrolled. If symptoms were present then mice were stratified according to severity of symptoms and randomly assigned into treatment groups. Mice were treated daily with either palbociclib or vehicle. Weights were recorded every 2 to 3 days. Humane euthanasia was performed during the study if mice demonstrated signs of tumor-related morbidity or lost more than 20% of body weight.

Target engagement

Mice bearing Med-211FH flank tumors were treated with palbociclib or vehicle. When tumors demonstrated evidence of

regression, mice were humanely euthanized approximately four hours after the last dose. Tissue was preserved by snap freezing and formalin fixation. Tumor tissue was suspended in RIPA buffer (Millipore) containing Halt protease inhibitors (Pierce Biotechnology) and PhoStop phosphatase inhibitors (Roche) and lysed using the TissueLyser II (Qiagen). Equal amounts of protein (100 μg) were loaded and resolved by SDS-PAGE using Nu-PAGE 4%–12% Bis-Tris gels (Invitrogen). Immunoblot was performed using standard techniques. Primary antibodies used were: Phospho-RB (Ser 780, #9307) and RB (#9309; Cell Signaling Technology, 1:1,000); and GAPDH (Santa Cruz Biotechnology, 1:500). Secondary antibodies used were: IRDye800CW Goat-anti-Mouse IgG and IRDye680LT Goat anti-Rabbit IgG (LI-COR). Membranes were scanned using LI-COR Odyssey. Image analysis was performed using Image Studio.

IHC

Samples were formalin-fixed, paraffin-embedded and sectioned at four microns. Antigen retrieval was performed using preheated pH 6.0 citrate buffer. Endogenous peroxidase activity was blocked using 3% H₂O₂ for eight minutes. Sections were blocked and stained with primary antibodies against phospho-Rb (Cell Signaling Technology, #8516, 1.21 μg/mL), Ki67 (Dako, #M7240, 0.8 μg/mL) for 60 minutes. Sections were incubated with either goat anti-rabbit HRP polymer (Biocare Medical, RHRP520L) for 30 minutes or goat anti-rabbit (Vector Laboratories, BA-1000) or goat anti-mouse (Vector Laboratories, BA-9200) biotinylated antibody followed by HRP reaction (Vector Laboratories, PK-6100). Staining was developed by 3,3'-diaminobenzidine (DAB+, Dako or Vector Laboratories) and sections counterstained with hematoxylin and mounted. Concentration-matched isotype controls were run for each tissue (Jackson ImmunoResearch Laboratories). Hematoxylin and eosin (H&E) staining was performed using standard procedures. Quantitation was performed using Halo v. 2.0.1038 (Indica Laboratories) digital pathology software. The percentage of tumor cells staining positive for the marker was determined using the cytonuclear algorithm: [(stain moderate cells + stain strong cells)/total cells] × 100. Quantitation was performed across the whole tumor section, excluding regions of necrosis.

Cell-cycle analysis

Mice bearing Med-211FH flank tumors were treated with palbociclib or vehicle for 10 days. Tumors were harvested at euthanasia and processed into a single-cell suspension. Cells were counted using Vi-Cell (Beckman Coulter) and resuspended in PBS containing 0.5% FBS. Two microliters (4×10^6 cells) was pipetted into 8 mL of ice-cold 70% ethanol and incubated at –20°C overnight for fixation and permeabilization. Cells were rehydrated and stained with propidium iodide before flow cytometry. Analysis was performed using FlowJo software.

MRI

Mice were enrolled when they developed signs of Med-211FH brain tumor development (mild to moderate head bulge) and assigned to palbociclib or vehicle treatment.

MRI was performed using a 1 Tesla (T) Bruker ICON mouse imaging system (Aspect Imaging, Shoham, Israel) every 2 to 4 days for 29 days. Ten-slice T1 and T2-weighted images were acquired for each mouse before intravenous injection with 0.3 mmol/kg gadopentetate dimeglumine (Magnevist, Bayer Healthcare).

T1 and T2-weighted images were acquired again postcontrast with a delay of 10–20 minutes.

T1-weighted imaging parameters: repetition time (TR) 159.466 ms, echo time (TE) 3.545 ms, acquisition matrix 0\89\89\0, flip angle of 80 degrees, field-of-view 30 mm, thickness 1 mm, and averages 3. T2-weighted imaging parameters: repetition time (TR) 4000.000 ms, echo time (TE) 50.00 ms, field-of-view 30 mm, thickness 1 mm, acquisition matrix 0\256\256\0, flip angle of 90 degrees and averages 3.

For quantitative analysis, all ten 2D T2-weighted postcontrast images from each mouse per acquisition were analyzed. Tumor volume was interactively identified by a reviewer (M.W. Nakamoto) using manual delineation of structures in 2D with ITK-SNAP segmentation software (28).

Bioinformatics

Expression data for 285 human medulloblastoma samples was downloaded from the Gene Expression Omnibus (GEO; GEO accession no. GSE37382). These expression data were generated on the Affymetrix Human Gene 1.1ST Array (GEO accession no. GPL11532). Expression data and sample annotation were extracted from the GSE37382 Series Matrix file. Data from GEO were \log_2 transformed and z-score normalized using R. Differential expression was calculated using the LIMMA package in Bioconductor. A threshold of 0.05 was applied to the Benjamini-Hochberg corrected P value to identify significantly differentially expressed genes relative to normal fetal and adult cerebellum. The local protein interaction network for CDKN2A was built using interactions from a manually curated human protein-protein interaction dataset (29). This dataset is derived from a manually curated knowledgebase incorporating information from human interactomes. Each interaction is systematically reviewed and curated from experimentally validated direct protein interactions characterized in the biomedical literature. The network was loaded into Cytoscape (30) and expression data were imported to identify overexpressed genes present in the network. Genes without significant differential expression were removed.

Statistical analysis

Tumor measurements from PDX flank tumor studies were analyzed using linear mixed models analysis in R. GraphPad Prism 7.0a software was used to analyze cell cycle and IHC data using the unpaired t test, and survival data using log rank (Mantel-Cox) test. Five mice were used in pilot studies to estimate population variance and observe a significant ($P < 0.05$) difference in sample means between treatments. For efficacy in brain tumors, a power analysis based upon historical data with median survival time (15 days) and SD (2.5 days) estimated that groups of 12 mice would detect survival differences greater than 1.2 SDs (~ 3 days) with 80% power in a two-sided test with 0.05 level of significance. Enrichment of differentially expressed genes in the local neighborhood of CDKN2A was analyzed using the hypergeometric distribution function in R. Genes were considered overexpressed if they had a \log_2 fold change (FC) > 1 and an adjusted P value of < 0.05 .

Results

Local network of CDKN2A reveals CDK6 as a novel therapeutically targetable node for all non-WNT medulloblastomas

Given that transposon-mediated inactivation of *Cdkn2a* cooperated with haploinsufficiency of *Ptch1* to increase incidence and

accelerate the development of medulloblastoma (13), we proposed that the underlying molecular interaction networks perturbed as a consequence of *Cdkn2a* inactivation may encompass a number of novel drug targets that, when blocked, are effective in halting tumorigenesis. To identify novel therapeutic targets that facilitate antitumor effect via CDKN2A, a local protein-protein interaction network was constructed for CDKN2A consisting of 149 proteins in total. On the basis that most drugs block protein function not augment it, the CDKN2A protein interaction network was refined to contain only the significantly overexpressed genes for SHH, group 3 and group 4 medulloblastoma ($P < 0.05$, FC > 0). The CDKN2A local network is strongly enriched for overexpressed genes in SHH ($P = 7.7 \times 10^{-6}$), group 3 ($P = 0.001$), and group 4 ($P = 0.004$) medulloblastoma. CDKN2A-interactor proteins were ranked on the basis of fold change (FC) for each subgroup, with the druggability of the top ten most overexpressed CDKN2A-protein interactors for each subgroup assessed by searching a database for known drug-target interactions (31). For SHH medulloblastoma, three significantly overexpressed CDKN2A-interactors were identified as potential therapeutic targets, including CDK6 ($P = 5.92 \times 10^{-8}$, FC = 2.32), Tumor Protein P53 (TP53; $P = 5.27 \times 10^{-8}$, FC = 1.68), and Aurora Kinase A (AURKA; $P = 6.69 \times 10^{-12}$, FC = 1.51; Fig. 1A). Two significantly overexpressed CDKN2A-interactor proteins were identified as therapeutic targets for group 3 medulloblastoma, including CDK6 ($P = 2.59 \times 10^{-06}$, FC = 1.86) and V-Myc Avian Myelocytomatosis Viral Oncogene Homolog (MYC; $P = 0.01$, FC = 1.62; Fig. 1B), whereas CDK6 was identified as the only significantly overexpressed druggable CDKN2A-interacting protein for group 4 medulloblastoma (Fig. 1C). Given CDK6 was identified as a significantly overexpressed druggable CDKN2A-interacting protein across all three subgroups of MB, blocking this kinase with a CDK4/6 inhibitor such as palbociclib is anticipated to be efficacious for all three subgroups of medulloblastoma.

Palbociclib suppresses Rb phosphorylation and causes G₁ arrest in Med-211FH patient-derived medulloblastoma subcutaneous tumors

Palbociclib was administered to mice bearing patient-derived MYC-amplified medulloblastoma tumors (Med-211FH) to determine whether the drug would inhibit RB phosphorylation and induce G₁ arrest. Initial studies involving palbociclib administration for 3 days and tumor resection 24 hours later failed to demonstrate any change in RB phosphorylation. Subsequent experiments involved administration of drug until tumors started to regress and resection at 4 hours after the last dose. These tumors demonstrated reduction in RB phosphorylation at Ser⁷⁸⁰ following treatment with palbociclib (Fig. 2A). There was a parallel decrease in total Rb that has been observed previously (22), but the mechanism is unknown. IHC staining confirmed significant inhibition of RB phosphorylation at Ser^{807/811} in palbociclib-treated tumors (Fig. 2C and D) as compared with vehicle (Fig. 2B and D). In further support of target engagement, palbociclib-treated tumors had higher accumulation of cells in the G₁ phase (97% of cells) as compared with vehicle-treated tumors (80% of cells, $P = 0.0005$; Fig. 2E and F; Table 1).

Palbociclib causes significant regression of SHH and group 3 patient-derived medulloblastoma subcutaneous tumors

Efficacy of palbociclib was tested in mice bearing PDX subcutaneous tumors representing two different subgroups of

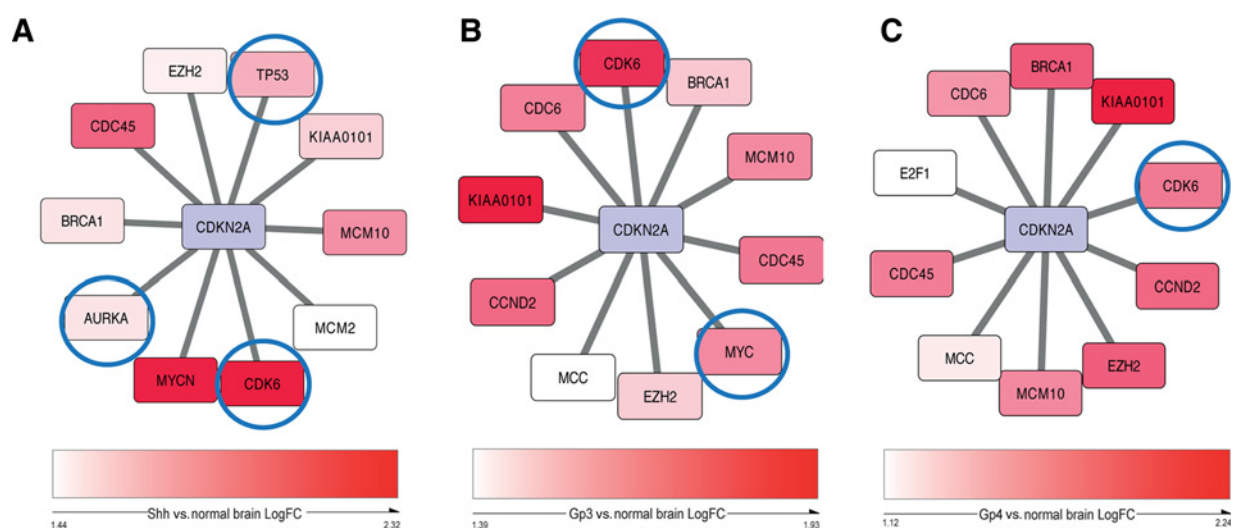


Figure 1.

CDK6 is a significantly overexpressed “druggable” CDKN2A-interacting protein identified across all non-WNT MB subgroups. Local direct protein–protein interactors of CDKN2A that are in the top 10 significantly overexpressed genes in SHH MB (A), Group 3 MB (B), and Group 4 MB (C). Nodes are colored on a red to white scale representing their expression in that respective subgroup, with red representing significantly overexpressed and white underexpressed. Nodes circled in blue represent molecular targets for drugs identified from Drugbank.

medulloblastoma: *MYC*-amplified group 3 (Med-211FH); and SHH (Med-1712FH). Palbociclib treatment resulted in tumor regression with an average reduction in tumor volume of 63% for both Med-211FH ($P = 0.001$, Fig. 3A) and Med-1712FH ($P = 1.14 \times 10^{-6}$, Fig. 3G); whereas growth continued at a high rate in vehicle-treated tumors, increasing in size by approximately 4-fold for Med-211FH and 2.7-fold for Med-1712FH.

Histologic analysis of palbociclib-treated Med-211FH and Med-1712FH flank tumors demonstrated significant reduction in cellularity with extensive fibrosis in addition to morphologic changes in both models (Fig. 3B, C, H, and I). Palbociclib-treated Med-211FH tumor cells demonstrated cytomegaly, prominent nucleoli, vacuolated chromatin, and indistinct cell borders (Fig. 3C). Med-1712FH drug-treated tumor cells demonstrated variable morphologic changes ranging from swollen with vacuolated cytoplasm and fading nuclei (karyolysis) to shrunken with condensed cytoplasm and hyperchromatic or fragmented nuclei (karyorrhexis; Fig. 3I). Med-211FH tumors had a relatively uniform response throughout the tumor, whereas Med-1712FH tumors had a heterogeneous response to palbociclib, with some portions of the tumor appearing similar to vehicle treatment (Fig. 3H).

Ki67 IHC staining was used to investigate the extent of proliferation in the tumors. Analysis of palbociclib-treated tumors indicated a reduction of approximately 84% in Ki67-positive tumor cells in Med-211FH tumors ($P < 0.0001$; Fig. 3E and F) and 32% in Med-1712FH tumors ($P = 0.02$; Fig. 3K and L) as compared with vehicle treatment (Fig. 3D and J). Interestingly, a proportion of the tumor cells remaining within the scar tissue in both models were positive for Ki67, indicating continued proliferation in drug-resistant cells.

Med-211FH subcutaneous tumors recur when palbociclib treatment is withdrawn

A definitive study was conducted to assess the extent of tumor regression in response to palbociclib and the frequency of tumor

recurrence following drug withdrawal in Med-211FH tumors. All drug-treated tumors regressed to the point where they could no longer be measured ($P < 1.0 \times 10^{-17}$) whereas vehicle-treated tumors progressed at a high rate of growth, increasing in volume by approximately 2.8-fold (Fig. 4A). Following 16 days of treatment, palbociclib was withdrawn and mice were monitored for tumor regrowth. A total of 15 of 20 palbociclib-treated tumors recurred within 60 days of drug withdrawal (Fig. 4B).

Longitudinal MRI study demonstrates significant regression of Med-211FH intracranial tumors during palbociclib treatment

The efficacy of palbociclib in medulloblastoma flank tumors prompted experiments in mice harboring tumors in the cerebellar microenvironment using MRI analysis. During early stages of treatment, a large tumor was identified by the hyperintense signal throughout the cerebellum in a representative mouse from both palbociclib and vehicle treatment cohorts (Fig. 5C and E). During the late stages of treatment, the tumor size reduced significantly in the drug-treated mouse and the cerebellar architecture appears relatively intact (Fig. 5D). In the vehicle-treated mouse the tumor has increased significantly in size and has greatly disrupted the cerebellar architecture (Fig. 5F).

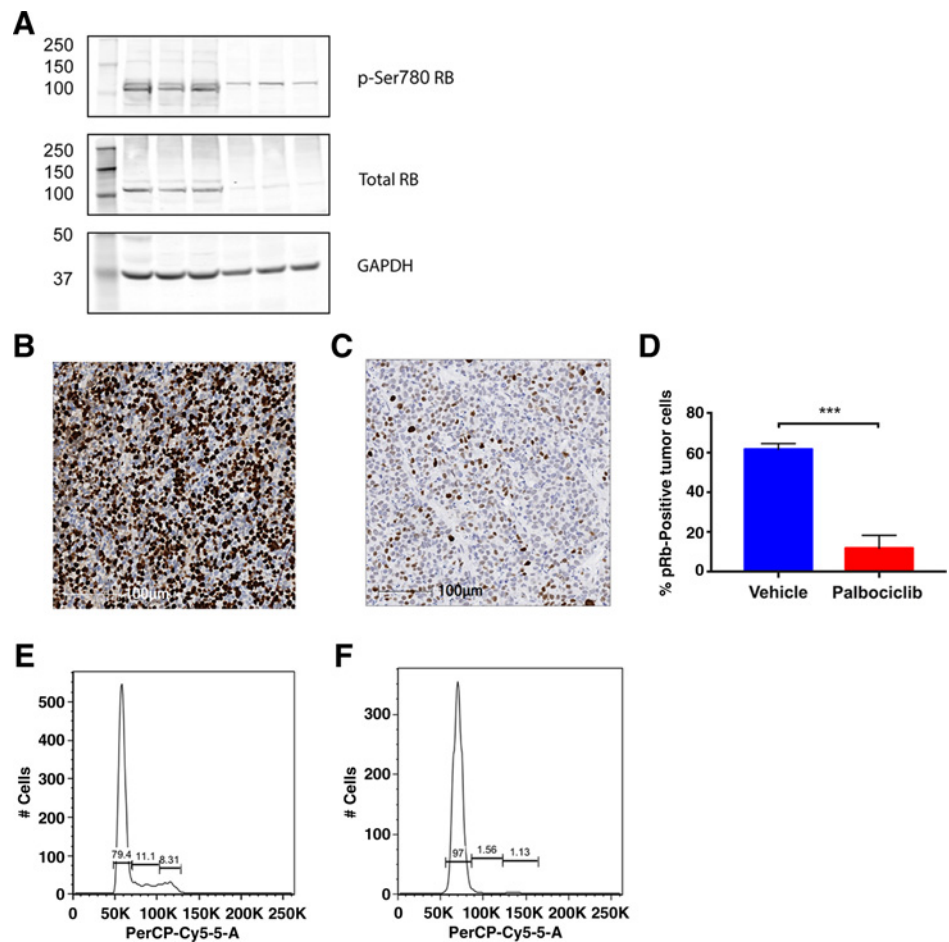
All palbociclib-treated mice survived for 29 days whereas the vehicle-treated mice were all euthanized because of tumor burden before the end of study (Fig. 5A). All tumors demonstrated enhancement in the presence of gadolinium contrast, suggesting that the blood–brain barrier (BBB) is compromised (Supplementary Fig. S2).

Palbociclib significantly increases survival in mice bearing orthotopic Med-211FH intracranial tumors

Definitive studies were conducted to investigate the efficacy of palbociclib in the treatment of *MYC*-amplified group 3 medulloblastoma brain tumors. After 31 days, 12 of 13 vehicle-treated mice had been euthanized because of tumor burden; however, all of the palbociclib-treated mice remained alive (Fig. 6A). Mice in

Figure 2.

Palbociclib engages its target following systemic treatment of mice bearing Med-211FH subcutaneous tumors. **A**, Immunoblot analysis of pSer 780 RB levels following treatment with vehicle or palbociclib. Blots were scanned using LI-COR Odyssey and images were processed and cropped using Image Studio and Adobe Photoshop, respectively. **B** and **C**, Representative images of pSer 807/811 RB immunostaining following vehicle (**B**) and palbociclib (**C**) treatment. **D**, Quantitative analysis of pSer Rb staining. The percentage of tumor cells staining positive were quantitated for vehicle ($n = 3$) and drug ($n = 3$) treated tumors using Halo software (Indica labs). Data are presented as the mean \pm SEM. Mean values were compared using an unpaired t test, $P = 0.0003$. **E** and **F**, Representative DNA histograms of subcutaneous tumors treated with vehicle (**E**) or palbociclib (**F**) and subjected to flow-cytometry analysis.



the drug-treated cohort were maintained on palbociclib for an additional 7 days and then a second phase of the trial was initiated in which the cohort was divided into two groups (Fig. 6B). In one group, drug treatment was maintained and in the other group drug was withdrawn. At the end of the trial, 4 of 5 mice in the drug-maintained group were alive, as compared with 1 of 5 mice in the drug-withdrawn group (Fig. 6B).

A follow-up study was performed to determine whether the survival benefit would extend to Med-411FH, another *MYC*-amplified group 3 tumor. At the end of the treatment period, all of the vehicle-treated mice had been euthanized because of tumor burden, whereas all of the palbociclib-treated mice remained alive (Fig. 6C). Despite the large difference in survival times, histologic analysis demonstrated significant tumor burden in both treat-

ment groups at the time of euthanasia and there was no significant difference in phospho-histone H3 levels. The most likely explanation for this finding is that dose reduction led to subtherapeutic drug concentrations between days 15 and 28.

Discussion

With the subdivision of medulloblastoma into four distinct molecular subclasses (10), it becomes important to identify and clinically test drug candidates that are tailored to relevant driver pathways. The paucity of patients available to enroll in clinical trials precludes statistically robust randomized trials of small subsets of patients. Therefore, the ideal drugs to advance to medulloblastoma patient clinical trials are those with relevance to multiple subclasses with priority given to agents that show activity in the poor prognosis tumor subtypes such as those with *MYC* amplification.

In this study, we hypothesized that the underlying regulatory networks perturbed as a consequence of *Cdkn2a* inactivation may encompass a number of novel drug targets that, when blocked, are effective in halting medulloblastoma tumorigenesis. A functionally defined protein interaction network identified the CDK4/6/ CYCLIN D/RB pathway as a novel therapeutic target in multiple medulloblastoma subclasses. Palbociclib, a selective inhibitor of CDKs 4 and 6, was predicted to be efficacious in medulloblastoma based upon bioinformatics analysis. *In vivo* studies in mice

Table 1. Palbociclib causes G₁ arrest in Med-211FH subcutaneous tumors

Treatment	G ₁ (% cells)	S (% cells)	G ₂ -M (% cells)
Vehicle 1	81.4	9.1	8.6
Vehicle 2	79.4	11.1	8.3
Palbociclib 1	95.5	2.2	1.2
Palbociclib 2	97	1.6	1.1
Palbociclib 3	97	1.9	0.7

NOTE: Quantitative analysis of DNA histograms generated by flow cytometry assessing the percentage of cells in each phase of the cell cycle in vehicle and palbociclib-treated subcutaneous tumors. The percentage of cells in G₁ phase were compared between palbociclib and vehicle treatment using unpaired t test ($P = 0.0005$).

Downloaded from <http://aacrjournals.org/clinccancerres/article-pdf/23/19/5802/2040672/5802.pdf> by guest on 26 August 2022

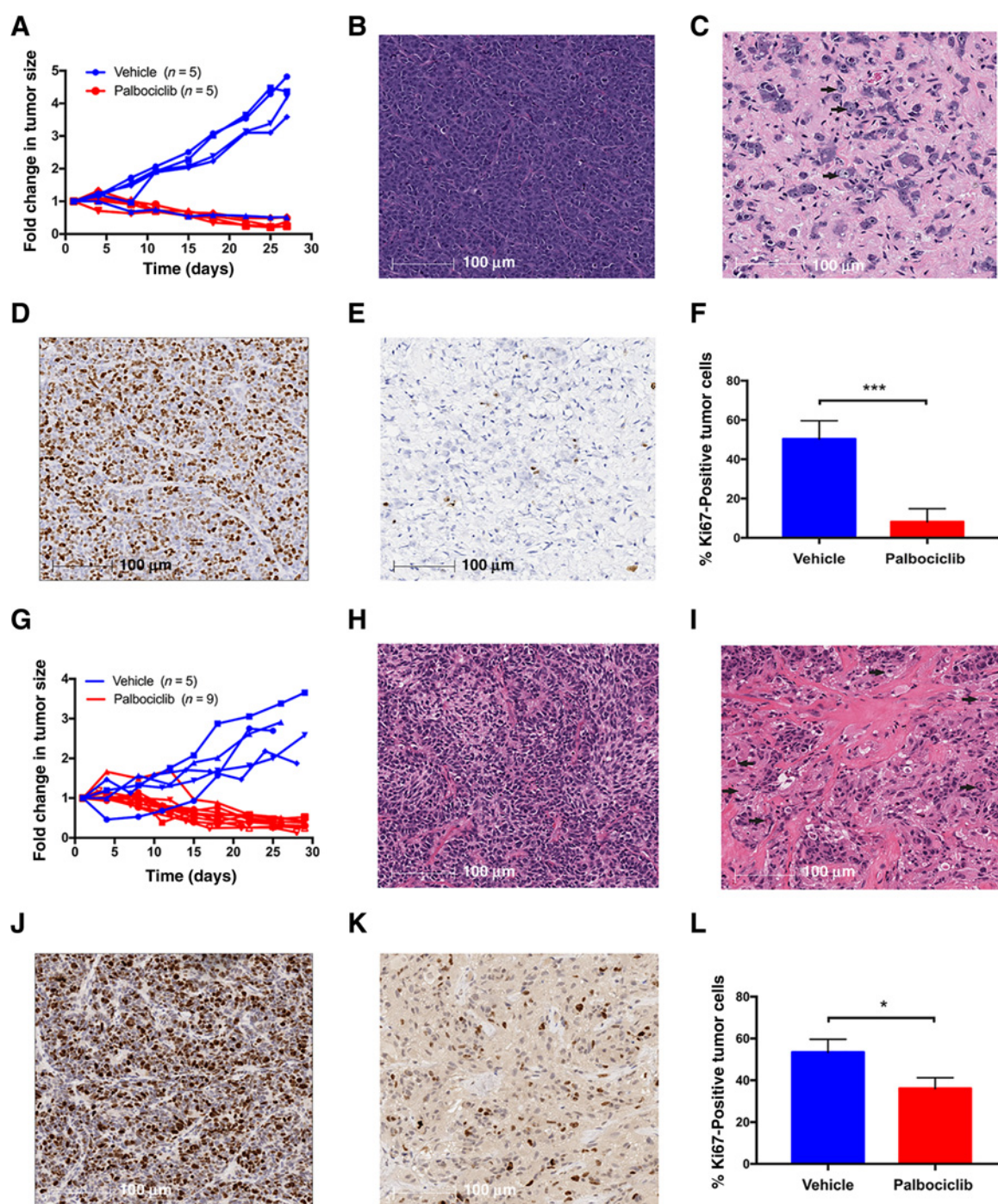


Figure 3.

Palbociclib causes regression of Group 3 and SHH medulloblastoma tumors. **A** and **G**, Fold change in tumor volume following treatment with palbociclib or vehicle in mice bearing Group 3 (Med-211FH, **A**) and SHH (Med-1712FH, **G**) medulloblastoma subcutaneous tumors for 28 days. Tumor measurements were compared between vehicle and drug treatments using linear mixed models analysis in R. **B**, **C**, **H**, and **I**, H&E sections demonstrating the effect of palbociclib on morphology of tumor cells in Med-211FH (**B**, **C**) and Med-1712FH (**H**, **I**) subcutaneous tumors following vehicle (**B** and **H**) and palbociclib (**C** and **I**) treatment. Arrows indicate cells that clearly demonstrate morphology change in response to drug treatment. **D**, **E**, **J**, and **K**, Representative images of Ki67 immunostaining as a marker of cell proliferation in Med-211FH (**D** and **E**) and Med-1712FH (**J** and **K**) subcutaneous tumors following vehicle (**D** and **J**) and palbociclib (**E** and **K**). **F** and **L**, Quantitative analysis of Ki67 staining in Med-211FH (**F**) and Med-1712FH (**L**) tumors. The percentage of tumor cells staining positive were quantitated for vehicle and drug-treated tumors ($n = 5$ each for Med-211FH and $n = 3$ each for Med-1712FH) using Halo software (Indica labs). Data are presented as the mean \pm SEM. Mean values were compared using an unpaired t test ($P < 0.0001$, Med-211FH and $P = 0.02$, Med-1712FH). One Med-211FH tumor-bearing mouse in the palbociclib treatment group required euthanasia on day 11 of the study for reasons unrelated to tumor growth.

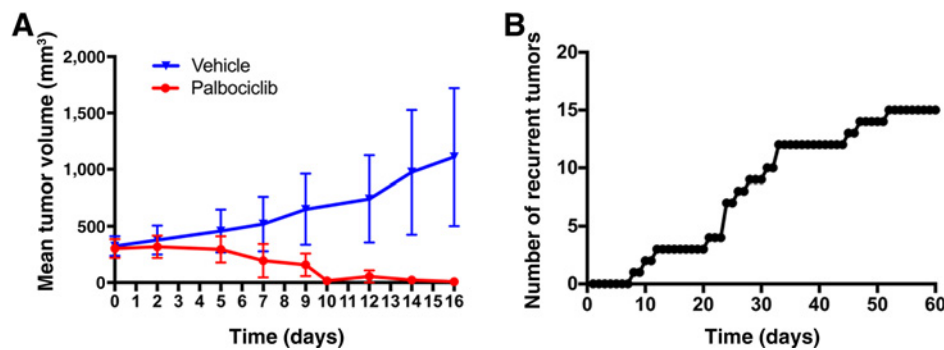


Figure 4.

Palbociclib causes complete regression of Med-211FH subcutaneous tumors, but drug withdrawal leads to tumor regrowth. **A**, Change in tumor volume following treatment with palbociclib ($n = 24$) or vehicle ($n = 18$) for 16 days in mice bearing Med-211FH subcutaneous tumors. Tumor measurements were compared between vehicle and drug treatments using linear mixed models analysis in R. Three vehicle-treated and 4 palbociclib-treated mice were euthanized following 9 days of treatment to confirm target engagement of the drug. **B**, Number of tumors that regrew over time following drug withdrawal. Palbociclib therapy was withdrawn, and mice ($n = 20$) were monitored for tumor regrowth. The time of tumor recurrence was recorded once tumor volume reached 100 mm³ or larger.

bearing PDX medulloblastoma subcutaneous tumors representing two different subgroups of medulloblastoma, *MYC*-amplified group 3 and *SHH* tumors, confirmed that palbociclib provides a significant therapeutic benefit in both subgroups. This was further confirmed in 2 different orthotopic brain tumor models of group 3 tumors in which the drug provided a highly significant survival benefit. We expect that similar efficacy would be observed in *SHH* subgroup brain tumors but this should be experimentally confirmed because of potential biological differences between tumors implanted in brain and flank.

The efficacy in two different *MYC*-amplified PDX brain tumor models is particularly striking given the aggressive nature of these tumors (5, 9, 10, 32, 33). *c-MYC* is a proto-oncogene that facilitates aberrant transition of cells through the G₁-S checkpoint via activation of CDK4/6/CYCLIN D complexes as well as CDK2/CYCLIN E (34, 35). It is possible that amplification of *MYC* works synergistically with aberrations in the CDK4/6/CYCLIN D/RB pathway in medulloblastoma to disrupt the G₁-S transition and make the cells dependent upon G₁ checkpoint defects for proliferation. A recently published study followed a similar experimental paradigm with implementation of a bioinformatics approach to identify CDK4/6/Cyclin D/Rb as a therapeutically relevant pathway for group 3 medulloblastoma, subsequently validating *in vivo* that palbociclib provides a survival benefit to mice bearing orthotopic xenografts of an established medulloblastoma cell line (36). Our work provides additional support for the importance of this pathway using an orthogonal bioinformatics approach, and extends the findings to demonstrate a significant survival benefit in mice bearing patient-derived medulloblastoma brain tumors that closely resemble the human tumors from which they were derived.

An important question is whether additional biomarkers, besides intact RB, could be used to focus medulloblastoma trials on patients who are most likely to respond. Unfortunately, no reliable biomarkers have been identified as evidenced by over 60 currently open palbociclib clinical trials that do not require amplifications/mutations of *CCN/CDK* or other pathway biomarkers for patient enrollment (clinicaltrials.gov). The reason for this is that a variety of epigenetic and genetic pathways converge on the *CCN/CDK/Rb* pathway to drive cancer. Thus, clinical trial

researchers are considering two options: (i) treating only medulloblastoma patients who have *CCN/CDK* amplifications or mutations as part of multicancer trials, such as the NCI-COG Pediatric MATCH precision medicine trial or (ii) enrolling a larger cohort of high risk, newly diagnosed patients in studies that require only intact RB. The latter is less efficient, but offers potential benefit to children who relapse due to a clone that involves this pathway or those with epigenetic-based RB pathway activation (21).

Based upon its mechanism of action, palbociclib is expected to cause cytostasis; however, the PDX medulloblastomas regressed extensively during treatment. This is consistent with previous reports from preclinical models and human clinical trials demonstrating regression of specific tumor types (22, 37–41). The mechanism for this is unknown. A cytostatic drug could cause tumor regression by inducing senescence in tumor cells (42). CDK4/6 inhibitors have been shown to act as epigenetic modulators enabling activation of senescence and potentially autophagy in tumor cells (43). Senescent cells release proinflammatory cytokines leading to elimination of tumor cells by phagocytosis (44).

An alternate explanation for tumor regression is that inhibition of CDKs 4 and 6 may be synthetically lethal in combination with specific oncogenic alterations. Notch1-induced T-cell acute lymphoblastic leukemias (T-ALL) and *MYC*-induced Burkitt lymphomas both undergo apoptosis in response to palbociclib therapy, whereas HER-2-positive breast tumors and K-Ras-induced non-small cell lung tumors both become senescent in response to palbociclib (37–39, 45). It is possible that *MYC* overexpression and *CDK6* amplification, which occur commonly in group 3 medulloblastomas (5, 11, 12), make the cells susceptible to cell death in response to palbociclib. In addition, palbociclib has recently been found to have pleiotropic effects, including inhibition of protein kinases, such as casein kinase 2 and PIK3R4, and several lipid kinases, through which it could induce autophagy or other forms of cell death (46).

It is notable that inhibition of RB phosphorylation was evident only at early timepoints after treatment. This indicates that the tumor cells are released from the effect of palbociclib within the dosing interval. Previous studies have demonstrated that the half-life of palbociclib in mice is 1.5 to 2 hours (47, 48), whereas in

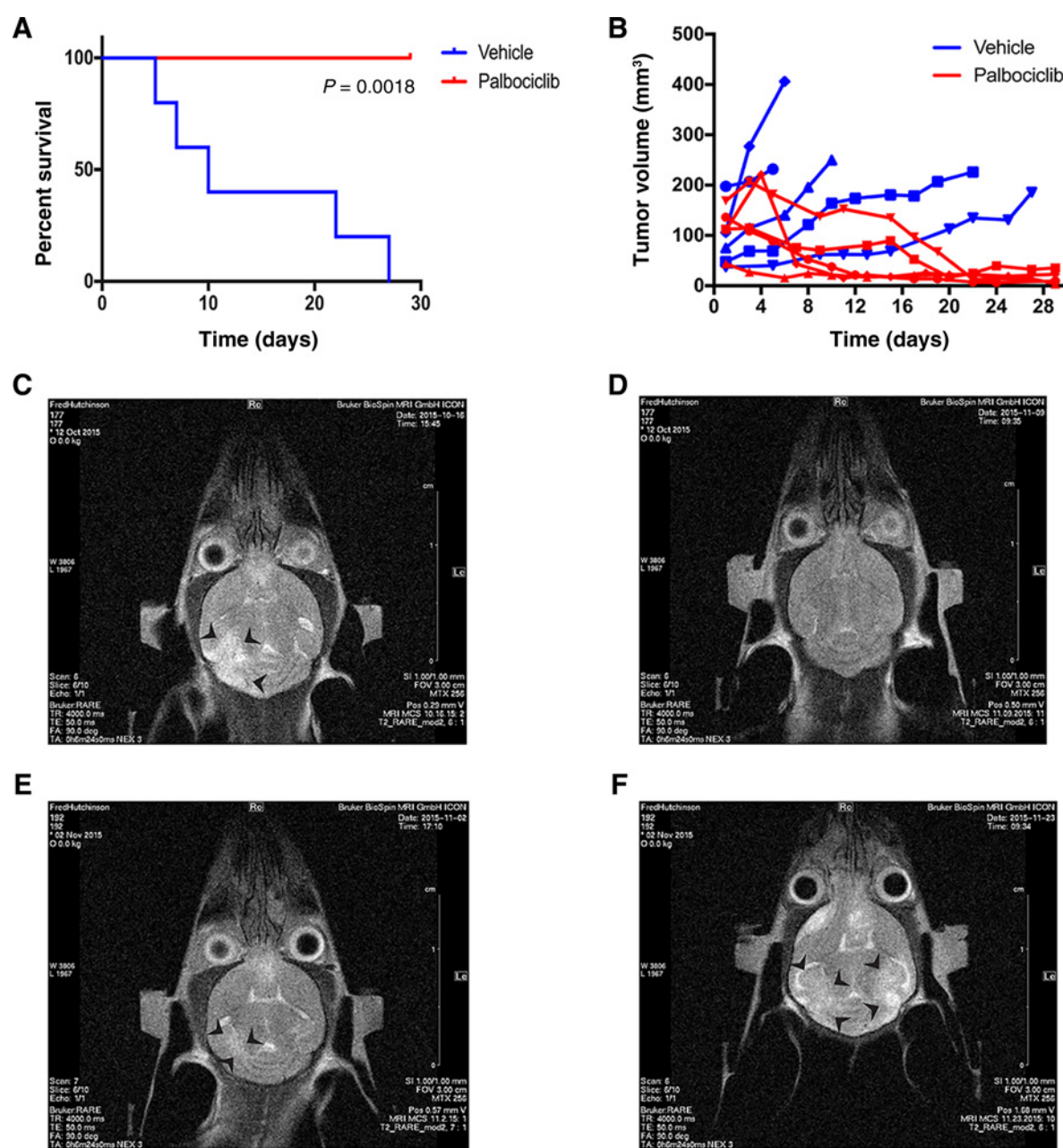


Figure 5.

Longitudinal MRI study demonstrates that palbociclib causes significant regression of Med-211FH brain tumors. **A**, Kaplan-Meier curve representing survival of mice bearing Med-211FH brain tumors that were treated with palbociclib ($n = 5$) or vehicle ($n = 5$) and serially imaged by MRI over the course of treatment. **B**, Change in tumor volume following treatment with vehicle or palbociclib. Tumor volume was measured using manual segmentation analysis of T2 post-gadolinium images in ITK-SNAP (38). **C** and **D**, Representative T2-weighted post-gadolinium MRI images for a palbociclib-treated tumor at early (**C**) and late (**D**) stages of treatment. **E** and **F**, Representative T2-weighted post-gadolinium MRI images for a vehicle-treated tumor at early (**E**) and late (**F**) stages of treatment. Arrows indicate the hyperintense tumor tissue in the cerebellum. The location of the tumor in each MR image has been highlighted in red in Supplementary Fig. S1.

humans it is 26.7 hours (26). Therefore, in humans, daily dosing provides exposure to the drug throughout the dosing interval, and leads to drug accumulation with repeated dosing (26). The difference in pharmacokinetic parameters between human and mouse could have a significant impact on response to palbociclib. Human clinical trials will be needed to determine whether the

intratumoral concentration required to cause tumor regression is achievable in human patients at the MTD.

There is clear evidence of tumor recurrence once palbociclib is withdrawn. It is possible that the resistant cells represent a small population present in the original tumor and form the basis for a clonal outgrowth in relapsed tumors. In practice, palbociclib will

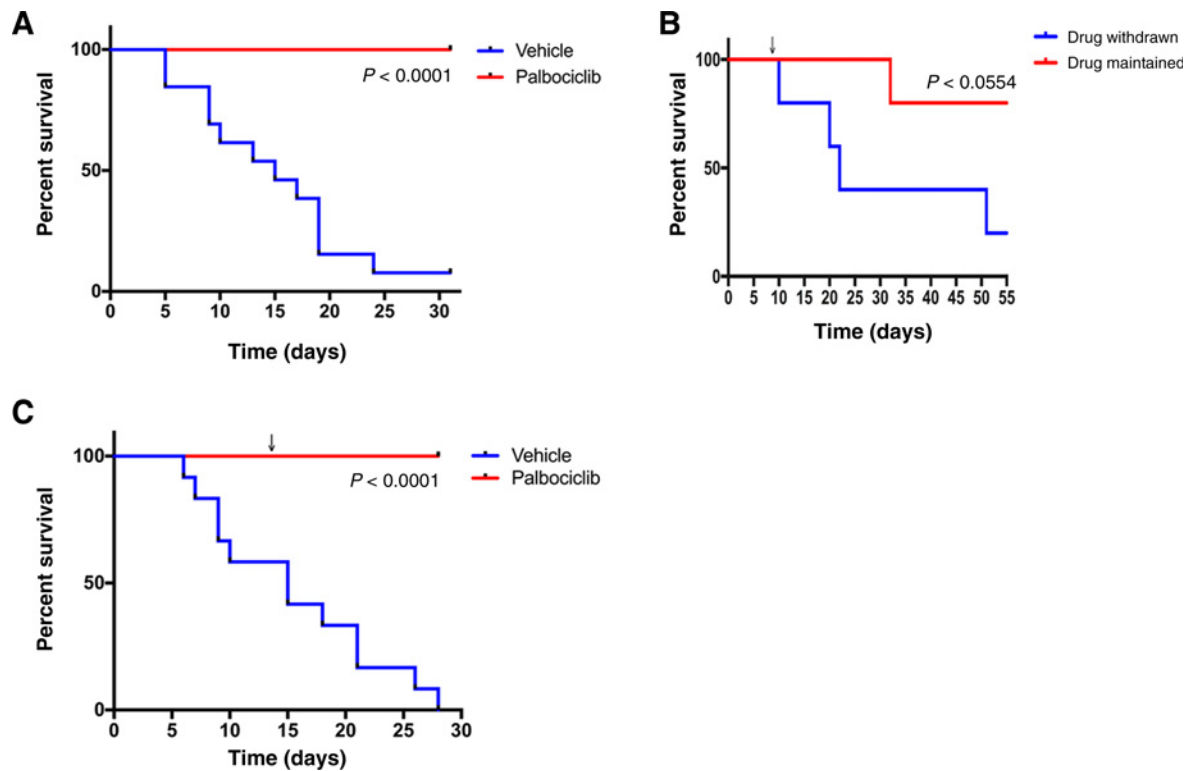


Figure 6.

Palbociclib significantly extends survival of mice bearing *MYC*-amplified medulloblastoma patient-derived orthotopic xenografts. **A** and **C**, Kaplan-Meier curves representing survival of mice bearing PDX medulloblastoma brain tumors from 2 different patients (Med-211FH and Med-411FH) following treatment with palbociclib or vehicle. **A**, Med-211FH tumors treated with either palbociclib ($n = 13$) or vehicle ($n = 13$). **C**, Med-411FH tumors treated with either palbociclib ($n = 12$) or vehicle ($n = 12$). Arrows indicate points at which dose was reduced by 50%, **B**, Kaplan-Meier curve representing survival of Med-211FH mice from the palbociclib treatment cohort that were enrolled into a second phase of the study on day 38. In this phase, 50% of the mice were maintained on drug ($n = 5$), and 50% were withdrawn from drug ($n = 5$). Arrows indicate points at which dose was reduced by 50% due to weight loss in the absence of appreciable signs of tumor development. The mice regained weight following the dose reduction.

unlikely be administered as a monotherapy, but as part of a drug combination that addresses the residual palbociclib-resistant cells.

Recent evidence has also emerged that palbociclib is a substrate for the drug efflux transporters P-glycoprotein and breast cancer resistance protein (48, 49), which are highly expressed on the BBB. MRI analysis indicated that there is loss of BBB integrity in the orthotopic tumors used in this study, which likely facilitated drug exposure. Many medulloblastomas have disrupted BBB and palbociclib might be considered for cytoreduction in these patients before surgery. BBB-penetrating CDK4/6 inhibitors, which are in development, would be necessary for activity against tumor cells protected by intact BBB.

The data presented here were used by the Pediatric Brain Tumor Consortium to launch a phase I clinical trial to test safety of palbociclib in patients with recurrent, progressive, or refractory central nervous system tumors (NCT02255461). Given that induction of p-glycoprotein pumps is a common mechanism of drug resistance, it is possible that patients with chemotherapy-naïve medulloblastoma would benefit more than those with refractory or recurrent disease. Provided that the current trial establishes safety of palbociclib in pediatric patients, it may be prudent to deploy palbociclib as part of the postsurgery, post-

radiation chemotherapy cycle in newly diagnosed medulloblastoma patients.

Disclosure of Potential Conflicts of Interest

No potential conflicts of interest were disclosed.

Authors' Contributions

Conception and design: M.L. Cook Sangar, B.J. Wainwright, J.M. Olson
Development of methodology: M.L. Cook Sangar, M.W. Nakamoto, M.J. Davis
Acquisition of data (provided animals, acquired and managed patients, provided facilities, etc.): M.L. Cook Sangar, M.W. Nakamoto, P. Ji
Analysis and interpretation of data (e.g., statistical analysis, biostatistics, computational analysis): M.L. Cook Sangar, L.A. Genovesi, M.W. Nakamoto, M.J. Davis, S.E. Knobluagh, B.J. Wainwright, J.M. Olson
Writing, review, and/or revision of the manuscript: M.L. Cook Sangar, L.A. Genovesi, M.W. Nakamoto, M.J. Davis, S.E. Knobluagh, B.J. Wainwright, J.M. Olson
Administrative, technical, or material support (i.e., reporting or organizing data, constructing databases): M.W. Nakamoto, A. Millar
Study supervision: M.L. Cook Sangar, J.M. Olson

Acknowledgments

The authors would like to thank patients and families who contributed brain tumor tissue for the PDX models, Pfizer Global Health for providing palbociclib, and Kyle Pedro, Emily Girard, Experimental Histopathology, and Comparative Medicine for their contributions to the work.

Grant Support

This work was supported by NIH/NCI RO1 CA112250 (to J.M. Olson); NIH/NCI RO1 CA135491 (to J.M. Olson); Seattle Children's Brain Tumor Endowment (to J.M. Olson); the Kids Cancer Project (to B.J. Wainwright); the Cure Brain Cancer Foundation (to B.J. Wainwright); and the Brainchild Foundation (to B.J. Wainwright).

References

- Leary SE, Olson JM. The molecular classification of medulloblastoma: driving the next generation clinical trials. *Curr Opin Pediatr* 2012;24:33–9.
- Mulhern RK, Palmer SL, Merchant TE, Wallace D, Kocak M, Brouwers P, et al. Neurocognitive consequences of risk-adapted therapy for childhood medulloblastoma. *J Clin Oncol* 2005;23:5511–9.
- Gajjar A, Chintagumpala M, Ashley D, Kellie S, Kun LE, Merchant TE, et al. Risk-adapted craniospinal radiotherapy followed by high-dose chemotherapy and stem-cell rescue in children with newly diagnosed medulloblastoma (St Jude Medulloblastoma-96): long-term results from a prospective, multicentre trial. *Lancet Oncol* 2006;7:813–20.
- Kool M, Jones DT, Jager N, Northcott PA, Pugh TJ, Hovestadt V, et al. Genome sequencing of SHH medulloblastoma predicts genotype-related response to smoothened inhibition. *Cancer Cell* 2014;25:393–405.
- Northcott PA, Korshunov A, Witt H, Hielscher T, Eberhart CG, Mack S, et al. Medulloblastoma comprises four distinct molecular variants. *J Clin Oncol* 2011;29:1408–14.
- Northcott PA, Nakahara Y, Wu X, Feuk L, Ellison DW, Croul S, et al. Multiple recurrent genetic events converge on control of histone lysine methylation in medulloblastoma. *Nat Genet* 2009;41:465–72.
- Thompson MC, Fuller C, Hogg TL, Dalton J, Finkelstein D, Lau CC, et al. Genomics identifies medulloblastoma subgroups that are enriched for specific genetic alterations. *J Clin Oncol* 2006;24:1924–31.
- Ahmed N, Ratnayake M, Savoldo B, Perlaky L, Dotti G, Wels WS, et al. Regression of experimental medulloblastoma following transfer of HER2-specific T cells. *Cancer Res* 2007;67:5957–64.
- Cho YJ TA, Tamayo P, Santagata S, Ligon A, Greulich H, Berhoukim R, et al. Integrative genomic analysis of medulloblastoma identifies a molecular subgroup that drives poor clinical outcome. *J Clin Oncol* 2011;29:1424–30.
- Taylor MD, Northcott PA, Korshunov A, Remke M, Cho YJ, Clifford SC, et al. Molecular subgroups of medulloblastoma: the current consensus. *Acta Neuropathol* 2012;123:465–72.
- Roussel MF, Robinson GW. Role of MYC in medulloblastoma. *Cold Spring Harb Perspect Med* 2013;3:pil014308.
- Northcott PA, Shih DJ, Peacock J, Garzia L, Morrissy AS, Zichner T, et al. Subgroup-specific structural variation across 1,000 medulloblastoma genomes. *Nature* 2012;488:49–56.
- Genovesi LA NC, Davis MJ, Remke M, Taylor MD, Adams DJ. Sleeping Beauty mutagenesis in a mouse medulloblastoma model defines networks that discriminate between human molecular subgroups. *Proc Natl Acad Sci U S A* 2013;46:E4325–E34.
- Sherr CJ, Roberts JM. CDK inhibitors: positive and negative regulators of G1-phase progression. *Genes Dev* 1999;13:1501–12.
- Lundberg AS, Weinberg RA. Functional inactivation of the retinoblastoma protein requires sequential modification by at least two distinct cyclin-cdk complexes. *Mol Cell Biol* 1998;18:753–61.
- Meyerson M, Harlow E. Identification of G1 kinase activity for cdk6, a novel cyclin D partner. *Mol Cell Biol* 1994;14:2077–86.
- Matsushime H, Ewen ME, Strom DK, Kato JY, Hanks SK, Roussel MF, et al. Identification and properties of an atypical catalytic subunit (p34^{PSK-J3}/cdk4) for mammalian D type G1 cyclins. *Cell* 1992;71:323–34.
- Marino S, Vooijs M, van Der Gulden H, Jonkers J, Berns A. Induction of medulloblastomas in p53-null mutant mice by somatic inactivation of Rb in the external granular layer cells of the cerebellum. *Genes Dev* 2000;14:994–1004.
- Zindy F, Nilsson LM, Nguyen L, Meunier C, Smeyne RJ, Rehg JE, et al. Hemangiosarcomas, medulloblastomas, and other tumors in Ink4/p53-null mice. *Cancer Res* 2003;63:5420–7.
- Mendrzyk F, Radlwimmer B, Joos S, Kokocinski F, Benner A, Stange DE, et al. Genomic and protein expression profiling identifies CDK6 as novel independent prognostic marker in medulloblastoma. *J Clin Oncol* 2005;23:8853–62.
- Tamayo-Orrego L, Wu CL, Bouchard N, Khedher A, Swikert SM, Remke M, et al. Evasion of cell senescence leads to medulloblastoma progression. *Cell Rep* 2016;14:2925–37.
- Fry DW, Harvey PJ, Keller PR, Elliott WL, Meade M, Trachet E, et al. Specific inhibition of cyclin-dependent kinase 4/6 by PD 0332991 and associated antitumor activity in human tumor xenografts. *Mol Cancer Ther* 2004;3:1427–38.
- Barton KL, Misuraca K, Cordero F, Dobrikova E, Min HD, Gromeier M, et al. PD-0332991, a CDK4/6 inhibitor, significantly prolongs survival in a genetically engineered mouse model of brainstem glioma. *PLoS ONE* 2013;8:e77639.
- Michaud K, Solomon DA, Oermann E, Kim JS, Zhong WZ, Prados MD, et al. Pharmacologic inhibition of cyclin-dependent kinases 4 and 6 arrests the growth of glioblastoma multiforme intracranial xenografts. *Cancer Res* 2010;70:3228–38.
- Cen L, Carlson BL, Schroeder MA, Ostrem JL, Kitange GJ, Mladek AC, et al. p16-Cdk4-Rb axis controls sensitivity to a cyclin-dependent kinase inhibitor PD0332991 in glioblastoma xenograft cells. *Neuro Oncol* 2012;14:870–81.
- Schwartz GK, LoRusso PM, Dickson MA, Randolph SS, Shaik MN, Wilner KD, et al. Phase I study of PD 0332991, a cyclin-dependent kinase inhibitor, administered in 3-week cycles (Schedule 2/1). *Br J Cancer* 2011;104:1862–8.
- Flaherty KT, LoRusso PM, Demichele A, Abramson VG, Courtney R, Randolph SS, et al. Phase I, dose-escalation trial of the oral cyclin-dependent kinase 4/6 inhibitor PD 0332991, administered using a 21-day schedule in patients with advanced cancer. *Clin Cancer Res* 2012;18:568–76.
- Yushkevich PA, Piven J, Hazlett HC, Smith RG, Ho S, Gee JC, et al. User-guided 3D active contour segmentation of anatomical structures: significantly improved efficiency and reliability. *Neuroimage* 2006;31:1116–28.
- Lynn DJ, Chan C, Naseer M, Yau M, Lo R, Sribrania A, et al. Curating the innate immunity interactome. *BMC Syst Biol* 2010;4:117.
- Shannon P, Markiel A, Ozier O, Baliga NS, Wang JT, Ramage D, et al. Cytoscape: a software environment for integrated models of biomolecular interaction networks. *Genome Res* 2003;13:2498–504.
- Wishart DS, Knox C, Guo AC, Shrivastava S, Hassanali M, Stothard P, et al. DrugBank: a comprehensive resource for in silico drug discovery and exploration. *Nucleic Acids Res* 2006;34:D668–72.
- Hermes J, Neidt I, Luscher B, Sommer A, Schurmann P, Schroder T, et al. C-MYC expression in medulloblastoma and its prognostic value. *Int J Cancer* 2000;89:395–402.
- Ellison DW, Kocak M, Dalton J, Megahed H, Lusher ME, Ryan SL, et al. Definition of disease-risk stratification groups in childhood medulloblastoma using combined clinical, pathologic, and molecular variables. *J Clin Oncol* 2011;29:1400–7.
- Obaya AJ, Kottenko I, Cole MD, Sedivy JM. The proto-oncogene c-myc acts through the cyclin-dependent kinase (Cdk) inhibitor p27(Kip1) to facilitate the activation of Cdk4/6 and early G(1) phase progression. *J Biol Chem* 2002;277:31263–9.
- Steiner P, Philipp A, Lukas J, Godden-Kent D, Pagano M, Mittnacht S, et al. Identification of a Myc-dependent step during the formation of active G1 cyclin-cdk complexes. *EMBO J* 1995;14:4814–26.
- Hanaford AR, Archer TC, Price A, Kahlert UD, Maciaczyk J, Nikkhah G, et al. DiSCoVERing innovative therapies for rare tumors: combining genetically accurate disease models with in silico analysis to identify novel therapeutic targets. *Clin Cancer Res* 2016;22:3903–14.
- Malumbres M. Cell cycle-based therapies move forward. *Cancer Cell* 2012;22:419–20.

38. Sawai CM, Freund J, Oh P, Ndiaye-Lobry D, Bretz JC, Strikoudis A, et al. Therapeutic targeting of the cyclin D3:CDK4/6 complex in T cell leukemia. *Cancer Cell* 2012;22:452–65.
39. Choi YJ, Li X, Hydbring P, Sanda T, Stefano J, Christie AL, et al. The requirement for cyclin D function in tumor maintenance. *Cancer Cell* 2012;22:438–51.
40. Leonard JP, LaCasce AS, Smith MR, Noy A, Chirieac LR, Rodig SJ, et al. Selective CDK4/6 inhibition with tumor responses by PD0332991 in patients with mantle cell lymphoma. *Blood* 2012;119:4597–607.
41. Dickson MA, Tap WD, Keohan ML, D'Angelo SP, Gounder MM, Antonescu CR, et al. Phase II trial of the CDK4 inhibitor PD0332991 in patients with advanced CDK4-amplified well-differentiated or dedifferentiated liposarcoma. *J Clin Oncol* 2013;31:2024–8.
42. Sherr CJ, Beach D, Shapiro GI. Targeting CDK4 and CDK6: from discovery to therapy. *Cancer Discov* 2016;6:353–67.
43. Acevedo M, Vernier M, Mignacca L, Lessard F, Huot G, Moiseeva O, et al. A CDK4/6-dependent epigenetic mechanism protects cancer cells from PML-induced senescence. *Cancer Res* 2016;76:3252–64.
44. Campisi J. Aging, cellular senescence, and cancer. *Annu Rev Physiol* 2013;75:685–705.
45. Puyol M, Martin A, Dubus P, Mulero F, Pizcueta P, Khan G, et al. A synthetic lethal interaction between K-Ras oncogenes and Cdk4 unveils a therapeutic strategy for non-small cell lung carcinoma. *Cancer Cell* 2010;18:63–73.
46. Sumi NJ, Kuenzi BM, Knezevic CE, Remsing Rix LL, Rix U. Chemoproteomics reveals novel protein and lipid kinase targets of clinical CDK4/6 inhibitors in lung cancer. *ACS Chem Biol* 2015;10:2680–6.
47. Smith D, Tella M, Rahavendran SV, Shen Z. Quantitative analysis of PD 0332991 in mouse plasma using automated micro-sample processing and microbore liquid chromatography coupled with tandem mass spectrometry. *J Chromatogr B Analyt Technol Biomed Life Sci* 2011;879:2860–5.
48. Parrish KE, Pokorny J, Mittapalli RK, Bakken K, Sarkaria JN, Elmquist WF. Efflux transporters at the blood-brain barrier limit delivery and efficacy of cyclin-dependent kinase 4/6 inhibitor palbociclib (PD-0332991) in an orthotopic brain tumor model. *J Pharmacol Exp Ther* 2015;355:264–71.
49. Raub TJ, Wishart GN, Kulanthaivel P, Staton BA, Ajamie RT, Sawada GA, et al. Brain exposure of two selective dual CDK4 and CDK6 inhibitors and the antitumor activity of CDK4 and CDK6 inhibition in combination with temozolomide in an intracranial glioblastoma xenograft. *Drug Metab Dispos* 2015;43:1360–71.